POAC'13
Espoo, Finland

Proceedings of the 22nd International Conference on
Port and Ocean Engineering under Arctic Conditions
June 9-13, 2013
Espoo, Finland

A STUDY OF MEASURED LINE LOAD LENGTHS AND MAXIMUM ICE LOADS ON MODEL SHIP HULL

Mikko Suominen[1], Pentti Kujala[1]

[1]Aalto University, Espoo, FINLAND

ABSTRACT

Dynamic ice fields increase the risks related to winter navigation. Dynamic ice fields can cause pressure to the sides of the ships and ships get stuck in ice. If the pressure increases, a rupture might occur and the hull damages. In the EU FP7 project called SAFEWIN the risks and impacts of compressive ice fields on ships are investigated. Within the project ice model tests are conducted in the ice basin of Aalto University with a tanker model in compressive ice fields. In the model tests, the added resistance and ice loads on the ship hull resulting from the compression are measured. For the ice load measurements the model ship hull is instrumented at bow shoulder and midship with conventional load sensors and tactile sensor sheets.

This paper focuses on the ice load measurements. Tactile sensor sheets have been criticized for not being able to capture the dynamic ice loading. However, the measurements show good correlation between the load sensors and tactile sensor sheets, as presented in this study. Furthermore, the measured line load lengths and maximum ice loads are studied. The line load study consists of the line loads occurring on the ship model's hull and the line load induced to the ice field.

INTRODUCTION

Dynamic and compressive ice increases ice resistance and ice loads on a ship's hull. Especially the loading at midship is increasing when compared with non-compressive cases. The loading at the midship also adds additional resistance and might stop the ship or in the worst case damage the hull.

Ice loads on ship hull measurements in a model scale are rare and the measurements in a compressive model ice field are even rarer. Helsinki University of Technology, Laboratory of Naval Architecture and Marine engineering, and Academy of Sciences in USSR, Institute for Problems in Mechanics conducted measurements in a compressive model ice field in a joint research project (Kujala et al., 1991). In the tests, the towing force, speed and maximum compressive ice forces at midship were recorded and studied in a level ice sheet, open channel, compressive level ice and compressive channel. The research conducted in the joint project was summarized by Riska et al. (1995), which presented an early method to estimate the additional resistance due to compression. In addition, an initial method for predicting ice loads at midship was presented.

Recently Kujala and Arughadhoss (2012) studied the ice loading on the model hull with tactile sensor sheets. In the paper, the crushing pressure on a ship's hull was analysed

statistically. The study with the pressure foils showed that the line load decreases at the bow and midship as a function of line load width.

In this paper, the measurement data obtained with the tactile sensor sheet and conventional load sensors on the model ship's hull are compared with each other. After the comparison, the effect of line load width on the average and maximum line load occurring on the model hull and the measured maximum pressure along the load line is studied. In addition, the line load induced to the ice sheet is studied and compared with the line load on model's hull measurements. Furthermore, the results of the earlier study on line load on a model ship's hull are compared with the results presented in this paper.

The data used in this paper is gathered from the same measurements as presented by Suominen and Kujala (2012). It was shown by Suominen and Kujala (2012) that in dynamic and compressive ice, the loading at the midship increases significantly and is similar to the bow shoulder. As the focus of this paper is in the line load measurements, the studies related to other measurement are left for future studies.

TEST SET-UP

The ice model tests were conducted in the multipurpose basin of Aalto University. The tests were conducted in a level ice sheet, compressive level ice, closing channel and open channel to study the added resistance and added loads resulting from compression in the ice field. The test programme consisted of six test series where the ice thickness and compression level were varied, see Table 1.

The tests were performed by towing the model with a winch across the basin with a constant speed of 0.5 m/s, see Figure 1. The first test of each test series was level ice tests with no compression, the second test was compressive level ice tests and the rest were closing and open channel tests. For the second test and the channel tests the model was moved to the other side of the basin. The basin has a moving bridge above it, which has pushing plates extending from side to side and can be used to push the ice sheet. The compression in the ice field was produced by pushing the ice sheet with these pushing plates.

The procedure in closing channel tests was similar with the compressive level ice test. The bridge started to close the channel by pushing the ice sheet between the model and the bridge, see Figure 1. The towing continued until the model reached the other side of the basin. Open channel tests were conducted after the ice sheet was unusable for closing channel tests. In closing channel tests, different closing speeds were used to simulate different compression levels. Closing speeds of 0.01, 0.02 and 0.03 m/s were used to simulate low, moderate and severe compression respectively. The test set-up is described in more detail in Suominen & Kujala (2012).

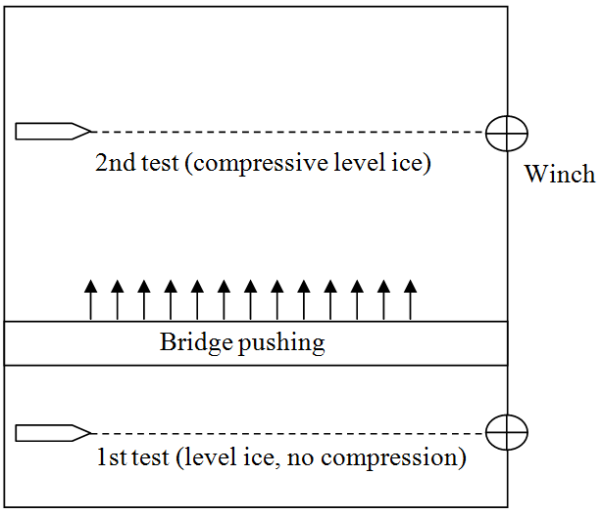

Figure 1. Layout of the test arrangement.

Table 1. Thickness and mechanical properties of ice, the closing speed of the channel and the ship model speed in the test series.

Test series number	Ice thickness [mm]	Mechanical properties (avg.) [kPa]		The used closing speeds of the channel [m/s]	The speed of the ship model [m/s]
		Bending str.	Compressive str.		
1	41	30.8	61.5	0.03	0.5
2	29	29.9	50.5	0.03	0.5
3	23	22.3	74.3	0.03	0.5
4	29	29.7	70.7	0.01, 0.02	0.5
5	29	29.5	56.5	0.01, 0.02, 0.03	0.5
6	24	22.9	69.9	0.01, 0.02, 0.03	0.5

INSTRUMENTATION OF THE MODEL

The model used in the tests is a model of 21 300 DWT general cargo carrier Credo designed by FKAB. The ship was chosen to represent a typical tanker / cargo vessel operating in the Baltic Sea as it has a Swedish-Finnish ice class of 1A Super and it has a long parallel midship section. The used model scale was 1:25.

Ice loads on the bow shoulder and the midship area were measured with load sensors and pressure foils. In order to measure ice loads with load sensors, two panels were cut out from the model and instrumented with load sensors, hereafter referred to as load panels. The dimensions of the load panels were 0.3 m * 0.2 m (width * height) at midship and 0.12 m * 0.2 m at bow shoulder. The centerline of the load panels in the vertical direction was at the water line. The pressure foils were then fixed with tape on top of the panels. Figure 2 presents the locations of the load panels and pressure foils.

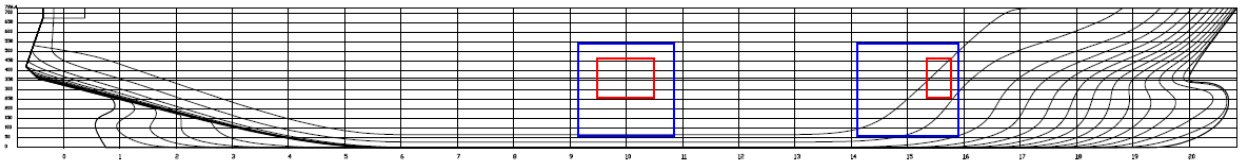

Figure 2. Locations of load panels and pressure foils. Inner red rectangles represent load panels and outer blue rectangles pressure foils.

The load panel at the bow shoulder was instrumented with one three-axial load sensor which measures loads in x-, y- and z-directions. Three-axial load sensor was chosen for ice load measurements at the bow shoulder as the hull of the model curves at this area meaning loads in different directions might occur. The load panel at the midship area was instrumented with three one-axial load sensors which were oriented to measure loads acting normal to the hull surface. All load sensors were calibrated with dead weights before mounting on the ship model. After the mounting of the sensor, additional calibrations were conducted with the load panels. The calibration is described in detail in Suominen and Kujala (2012).

The pressure foils used in the tests are part of a tactile sensor system called I-SCAN. The system consists of a sensor sheet, handle and measuring PC. The sensor sheet used in the tests is model 5350N. The width of the measuring area is 439.9 mm and the height is 480.1 mm. The sheet has 44 pressure cells to horizontal direction and 48 to vertical direction. The elements of the pressure foils have voids between each other. Each cell is a 10 mm by 10 mm square, with a 6 mm by 6 mm sensing area in the middle. Due to the voids, the actual measuring area of the pressure foil is 64% of the total element area. Before fixing the sheets to the model, the sheets were calibrated with dead weights at the temperature of 0^{o}C according to the system manual of Tekscan. Figure 4 presents an example of the time histories measured at the midship simultaneously with the pressure foil and the load panel.

The bridge above the basin has pushing plates which extend from side to side. The sides of the basin are 40 meters in length. In order to measure the force produced to the ice sheet, 10 m of this span was instrumented with load sensors. The centreline of the instrumented part was located 25 meters away from the starting side of the test runs. Load sensors were mounted between the pushing plates of the bridge and plates placed in front of these plates which were connected with hinges above, see Figure 3. Altogether four plates were placed in front of the pushing plates, each 2.4 m wide, and two load sensors were mounted on each plate.

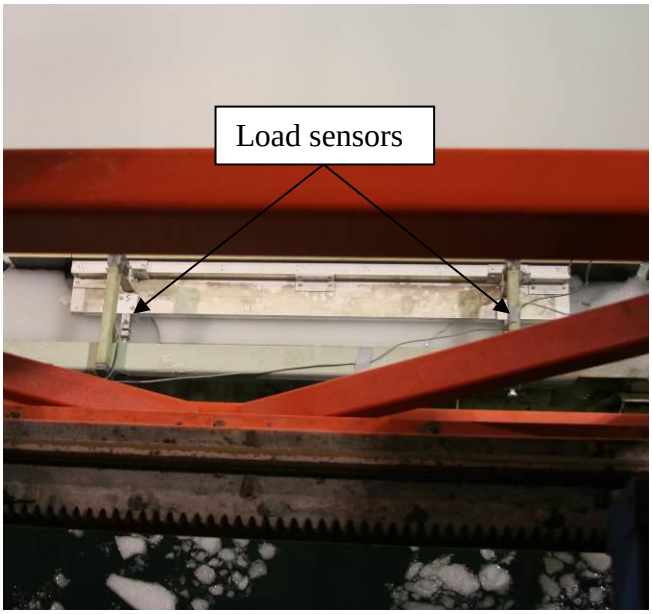

Figure 3. An instrumented pushing plates.

Figure 5 presents an example of the measured time histories with the pusher plates during the same test as presented in Figure 4. Line loads for separate pushing plates are determined by adding up the force measured with the two load sensors mounted on the same pusher plate

and then the force is divided by 2.4 meters. Total line load is calculated by adding up all the measured forces on pusher plates and the divided by 7.5 meters. It is assumed that the adjacent pusher plates carry the loading over the gap between the plates as the ice sheet is not broken. The pusher plates are numbered starting from the closest one to the starting point of the test. There were connection problems with a sensor mounted on the pusher plate number four and therefore it is left out from Figure 5.

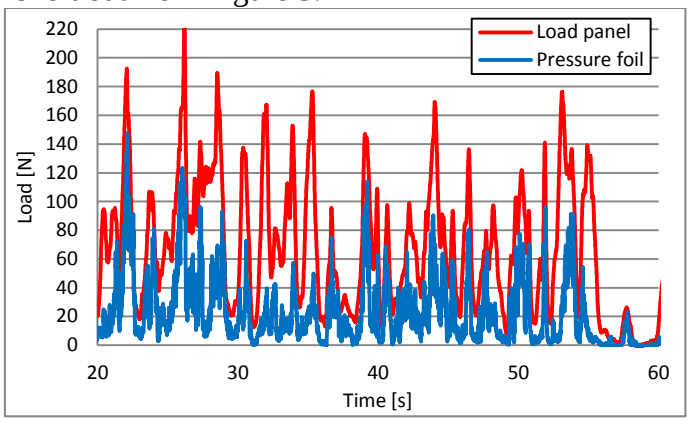

Figure 4. The time histories measured at the midship with the pressure foil and the load panel during the fourth test run in the second test series.

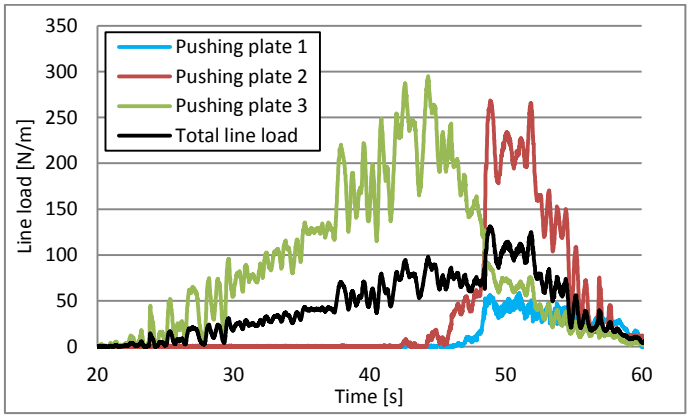

Figure 5. Time histories measured with the pusher plates separately and the calculated total line load during the fourth test run in the second test series.

In addition to the ice load on ship model hull and pusher plate measurements, the towing force of the winch was measured with a load sensor. The sensor was attached from one end to the bow of the model and to the towing rope from the other end. The study of the towing force is left for the future studies, as the focus of this paper is on the ice loading.

CORRELATION OF LOAD PANEL AND PRESSURE FOIL

For the purpose of validating the use of pressure foils the correlation between the data obtained from the load panels and the foils was calculated. A Pearson product-moment correlation coefficient was calculated for the data sets of each test using Excels built in CORREL-function. Spatial and temporal similarity between the data sets was needed to make the calculation meaningful.

The pressure foils covered a larger area than the load panels. Therefore the areas from which the measurement data with pressure foils was collected for correlation study, was reduced to the same area that was covered with the load panels. Some inaccuracy for the correlation study comes from the outer skirt of the panels as the foils cells could not form exactly the

same area as the panel. The sample frequencies of the plates and foils were different from each other. A sample rate of 100 Hz was used with the pressure foils while the rate was 123 Hz for the load plates. First the timestamps of the datasets were synchronized and then an algorithm picked values from the larger data set minimizing the time differences of samples with the same index. The time differences of data points with the same indexes were under 0,005 s in the matched sets.

The correlation coefficients were determined for the matched datasets and for sets containing averages and maxima for one and half second intervals. The intervals were used to see if there is a noticeable difference in the rate of response in the two sensor systems. The correlations were calculated for the midship and bow shoulder areas for all successful test runs. The calculated correlations for the panel and the foil at midship for the second test series are presented in Table 2. The color coding indicates the strength of the correlation; r>0,9 is shown as green, r=0,75 as yellow and r<0,5 as red. The interpretation of the correlation coefficient is somewhat arbitrary but a strong correlation should be expected as the sensors have measured the same phenomena.

Table 2: Pearson product-moment correlation coefficients for the midship area (on the top) and the bow shoulder area (the bottom one) for the second test series.

		Matched sampling frequencies	One second average values	One second maxima	Half second average values	Half second maxima
Test	Description	r				
2_1	Level ice	0.79	0.87	0.88	0.86	0.88
2_2	Compr. level ice, 0.002 m/s	0.90	0.95	0.95	0.95	0.93
2_3	Closing channel, 0.03 m/s	0.78	0.88	0.89	0.88	0.86
2_4	Closing channel, 0.03 m/s	0.73	0.86	0.83	0.81	0.82
2_5	Closing channel, 0.03 m/s	0.78	0.90	0.90	0.85	0.86
2_6	Closing channel, 0.03 m/s	0.82	0.96	0.92	0.92	0.91

Test	Description	r				
2_1	Level ice	0.69	0.78	0.84	0.77	0.80
2_2	Compr. level ice, 0.002 m/s	0.59	0.83	0.74	0.80	0.75
2_3	Closing channel, 0.03 m/s	0.55	0.72	0.78	0.71	0.77
2_4	Closing channel, 0.03 m/s	0.60	0.61	0.82	0.66	0.79
2_5	Closing channel, 0.03 m/s	0.56	0.81	0.82	0.77	0.79
2_6	Closing channel, 0.03 m/s	0.60	0.85	0.85	0.80	0.83

The study showed that the correlation is strong at midship with r≈0,9. The correlation is the poorest in the matched dataset and slightly stronger in one second intervals than at half second intervals. The data sets composed of the maximum values at time intervals and have a slightly stronger correlation than the average values of time intervals.

The cases of compressive level ice and closing channel show the strongest correlation with correlation decreasing slightly with increasing ice speed. The weakest correlations are in the

level ice tests and especially in the open channel tests, where the standard deviation is also the greatest. This could be due to the placement of the foil and panel. The foil is measuring the loading on the surface of the structure whereas the load sensors of the load panel are measuring loading behind the structure. In the level ice and open channel tests only a few minor loading occur at midship. The foil on the surface in these cases has contact with the ice field, but the load panel does not react to these loadings.

The calculated correlations for the panel and the foil at bow shoulder for the second test series are presented in Table 2. It can be seen that the correlation is significantly weaker than in the midship area. This might be due to the greater curvature in the bow shoulder area compared with the midship area which affects the performance of the pressure foil adversely. In addition the load panel at the bow shoulder is significantly smaller than at the midship, which increases the difference in the measurements resulting from the difference in the out skirt of the panel.

LINE LOAD ON MODEL HULL

In this chapter, the width of line load and occurring maximum ice loads are studied. The effect of the ice thickness and the level of compression to the ice loading on the model hull is not studied in this paper. Therefore only the measurement data from test runs 3 to 6 in the second test series is studied here as the ice thickness and compression level do not vary in the test series.

The measurement data used is gathered only with the pressure foils at the midship and bow shoulder. The whole area of the foils was used in the study excluding the outer skirt of the foil. The cells at the outer skirt were showing a constant pressure, which was due to the mounting of the foils from sides on the model hull. The largest usable area to examine data was determined by checking the test runs and excluding all elements that could not give reliable data for all test runs. The size of this area is the same for both the bow shoulder and midship sensors, but its location on the measuring area is slightly different. The edges of this "box" for all test runs can be seen in Table 3. Indexing for the element rows and columns starts from the top left corner of the matrix.

Table 3. The examined areas of the pressure foils.

	Bow shoulder	Midship
Top	11	4
Bottom	26	21
Left	2	2
Right	41	41

The time intervals used to analyze the data from pressure foils started when the channel began to close and ended when the stable towing force ends. The threshold for noise was set at 3 kPa in the measurements, and the saturation pressure was 221 kPa due to the sensitivity choice for the foils. The threshold level seems sufficient as there is no notable noise at the waterline when the summation of the "box area" is calculated.

Initial data processing

Both sensor foils were measuring with the sample rate of 100 Hz. For each time step or time frame the waterline is determined to be in a row that has the maximum total load. The

waterline row and both adjacent rows are then checked for load cases. A load case is determined to be all adjacent contact elements with a pressure above the set threshold level of 3 kPa. An example of a wide load case can be seen in Figure 6. Figure 6 also presents a 9 cell wide single load case separated from the wide load case using the method described below. Load cases that are cut off by the edge of the examined area are ignored for the purpose to ensure that only whole cases are taken into account.

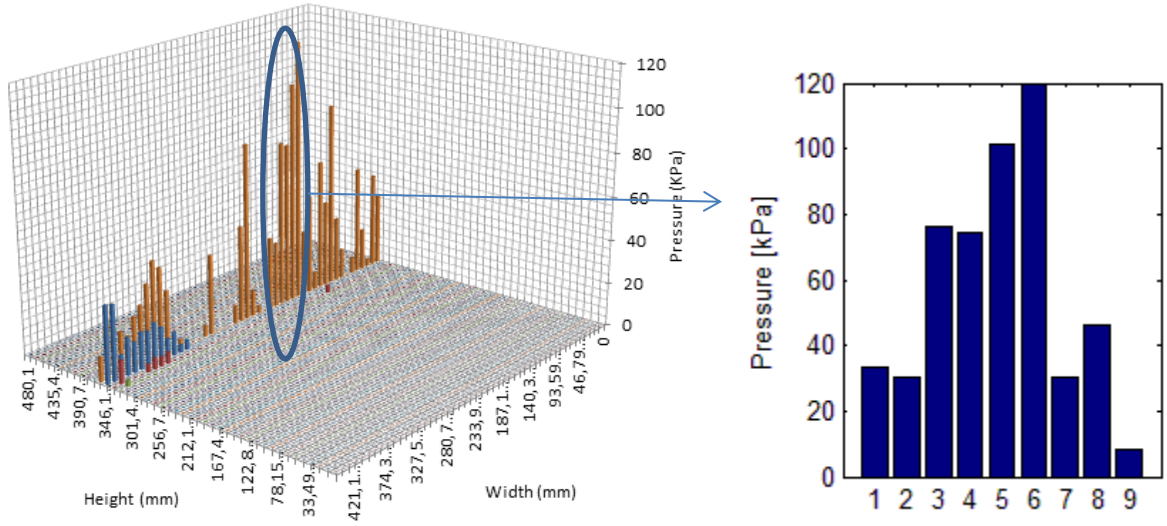

Figure 6. An example of a wide loading case at the midship at one time frame (on the left) and an example of a 9 cells wide single load case separated from the wide load case (on the right).

The total pressure for each time step is then calculated by summing all accepted load cases. Maximum loading events (local peak values in time history) are identified from the time history using Rayleigh criterion. Rayleigh criterion is used to identify separate peaks from a profile data. In order to accept two local maxima as separate peaks, the local minima between the maxima must be equal to or smaller than r times the value of the smaller maximum. The value of 1/5 for r is used in this case.

The relation for time in the ship and model scale can be derived from Froude's scaling to be

$$t_m = \frac{t_s}{\sqrt{\lambda}} \qquad (1)$$

where t is time, λ is the scaling factor and subscript s and m denote the ship and model scale respectively. Using Equation (1) and assuming that one loading case in full scale lasts 0.1seconds, it can be derived that one loading case would take 0.02 seconds in model scale, as the scaling ratio is 1:25. In order to ignore peaks that are too close in time history (the same loading case) the time between the accepted peaks was set to 0.05 seconds. This ensures that the same load case is not taken into account more than once. Figure 7 shows the time history of total load for the midship sensor in the 3rd test run at the 5th test series. In addition, Figure 7 illustrates which ice load peaks are accepted as short term maximum ice loads using Rayleigh separation without any threshold level.

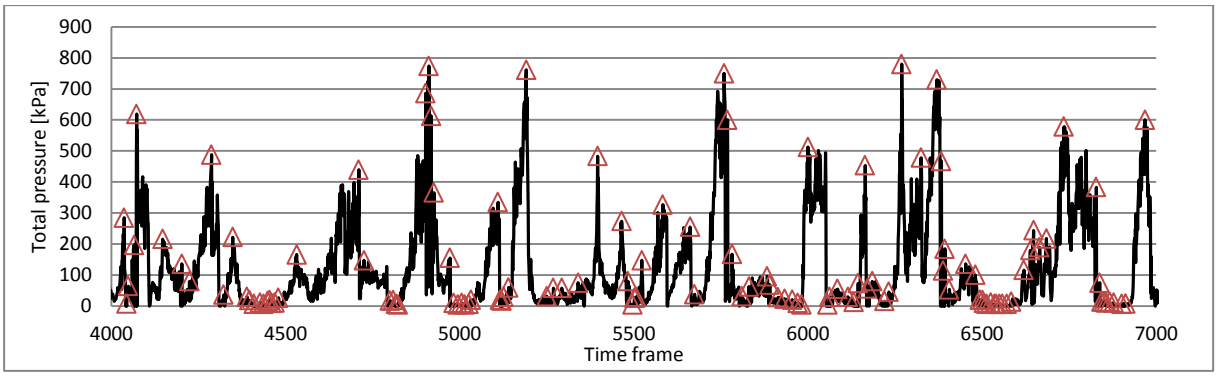

Figure 7. The measured total pressure on the foil as a function of time. Red triangular present the chosen maximum peak loads by using Rayleigh separation.

Wide loads that are likely to have more than one individual case are split by using Rayleigh criterion, see Figure 6. First, all peaks are identified using a Rayleigh parameter r = 1/3. The peaks must also have at least 3 cells between them to be considered as separate peaks. If two or more peaks can be found this way, the case is split into two or more smaller cases at the minimum value between the peaks. The minimum value is considered to belong to the left-hand case. An example of a separated load case from a split wide load case is presented in Figure 6. Rayleigh parameters used to split wide cases were intentionally set strict enough so that only obvious cases that consist of more than one individual load case were split into smaller cases. This ensures that the data remains reliable for smaller load lengths.

For the widest loads there always remains a small uncertainty whether it is caused by more than one individual event. Table 4 summarized how the total number of loading cases depends on the value of Rayleigh parameter, the number of cells between the split cases and the relative increase in the number of peaks in relation to the initial number of peaks with no splitting. The initial number of loading cases was 2028. As can be seen, the stricter the criterion the closer the final number of cases is to this initial number of non-split cases. With the parameters used in this study, the number of load cases is increased by about 9.5%.

Table 4. The effect of Rayleigh parameter and the minimum gap between the maximum load peaks. The data measured at midship in tests 3 to 6 in test series 2.

		Total number of peaks			Relative increase		
		The value of Rayleigh parameter			The value of Rayleigh parameter		
		0.5	0.33	0.25	0.5	0.33	0.25
Minimum gap between the picked maximum values with Rayleigh separation	2	2394	2304	2224	0.180	0.136	0.097
	3	2262	2221	2178	0.115	0.095	0.074
	4	2161	2159	2133	0.066	0.065	0.052

Figure 8 presents the effect of different threshold values to the number of ice load peaks. The load length is calculated from the number of load cells activated next to each other. As can be seen from Figure 8, the number of 0.01 meters wide load peaks is significantly higher when the threshold is 3 kPa. When the threshold is increased to 20 kPa the number of peaks in this class has reduced significantly, which indicates that the peaks in this class are small. On the opposite, the number of five cells wide loading cases is not sensitive to the threshold. This indicates that narrower loading width contains more small loads than wide cases.

Following the Froude's scaling laws, the pressure can be scaled from model scale to full scale as follows

$$p_s = p_m \lambda \quad (2)$$

where p denotes pressure, λ is scaling factor and the subscripts s and m represents ship and model scales. By using Equation (2) and taking into account the sensitive area of the cells, it can be determined that 5 kPa in the area of one cell corresponds to 12 kN in ship scale. Therefore the threshold is set to 5 kPa in order to reduce the possible noise and the magnitude of the threshold is at the same level as used earlier in the analysis of short term ice load measurements in full scale, see example Kujala et al (2009). The data measured with the pressure foil at the bow shoulder is processed with the same method. The number of load cases separated according to the contact width for the bow shoulder pressure foil is presented in Figure 9.

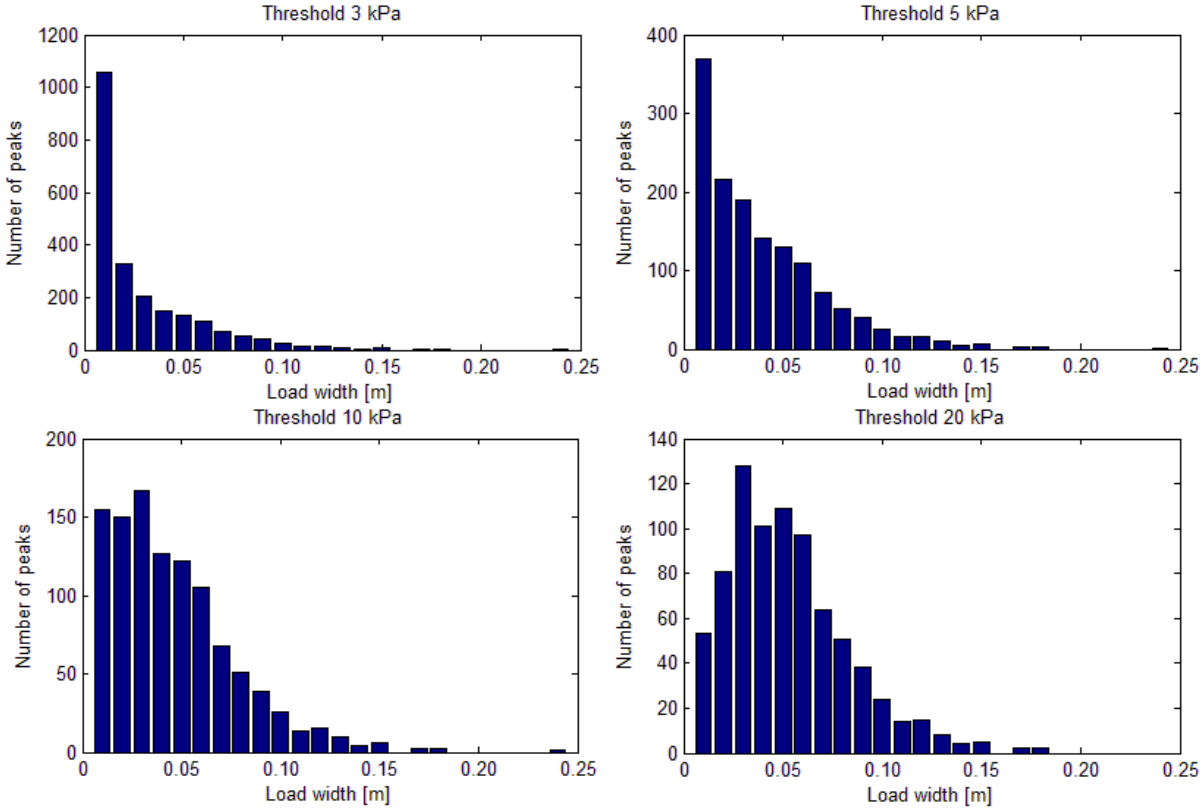

Figure 8. The effect of threshold value to the number of peaks at the midship in tests 3 to 6 in series 2.

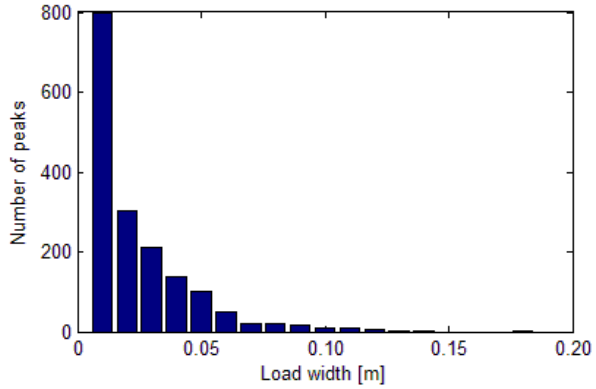

Figure 9. The number of loading cases as a function of contact width at the bow shoulder.

Line loads at the midship and bow shoulder

The number of load cases with different contact widths for the midship and bow shoulder pressure foil is presented in Figure 8 and Figure 9. The load cases are divided into load classes based on the contact length. For the line load calculation, the total force affecting on the contact line in a single loading case is calculated and then the average total force is calculated for each contact width, see Figure 10. The line load is then calculated by dividing the total force with the contact length. Figure 10 presents the average line load as a function of the contact width for the bow shoulder and midship for the load width intervals containing more than one loading case. Load width intervals containing only one loading case are not presented. As can be seen from Figure 10, the total force is increasing as a function of the contact width as expected. In addition, Figure 10 shows that the average line load is increasing as a function of the contact width until a width of 0.08 meters, after which it stabilizes and remains constant.

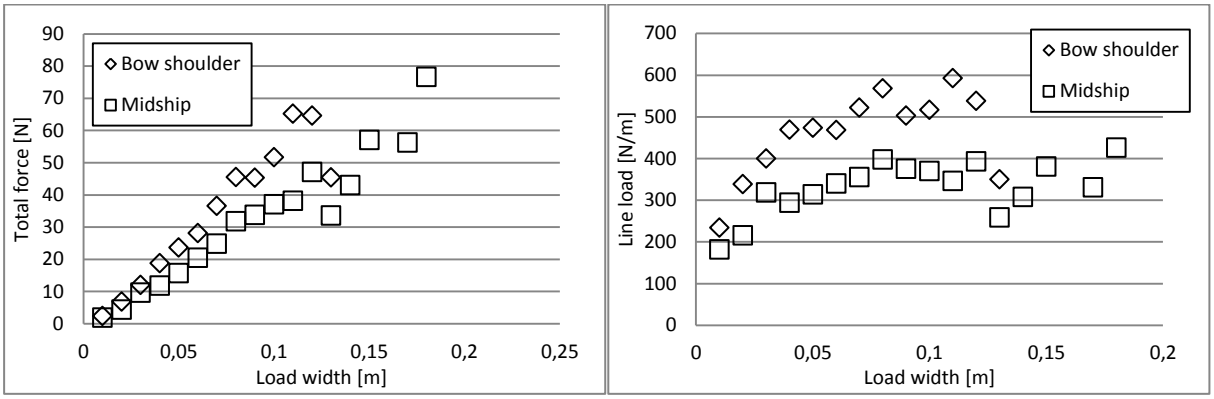

Figure 10. The average measured total forces in different load lengths (on the left) and the measured average line load as a function of the load width (on the right).

Figure 11 presents the maximum line load measured at the bow shoulder and midship as a function of loading width. In Figure 11, the maximum line load is determined by first defining the maximum pressure (the hot spot) from each loading case. The width of this loading case is 0.01 meters, which equals the width of the sensor. Then the width is expanded to the neighbourhood one sensor at the time (the width of the loading case increases 0.01 meters at each step) and the line load for the total contact width is calculated at each step. This is continued until the total width of the loading case is reached. After all the loading cases for different widths of line loads have been defined, the maximum line load for each loading width class is determined. Only the load width intervals containing more than one loading case are accepted for the study. As can be seen from Figure 11, the line load is decreasing as a function of contact width when the initial condition and contact length is chosen to be the length of the hot spot.

Curves were fitted to the data points of the bow shoulder and the midship, see the fitted lines in Figure 9, using the least mean square fit. The equation for the curved was of the form

$$q = C\left(\frac{l_c}{s}\right)^{-a} \quad (3)$$

where q is line load, C and a are unknown parameters, l_c is the contact length and s is the smallest load width obtained by scaling the typical full scale values of frame spacing to model scale. In a full scale, the typical values are around 350 mm (Kujala and Arughadhoss, 2012), which is 0.014 meters in the model scale used in this study. Table 5 presents the parameter values defined for the fitted curves for the bow shoulder and the midship and the coefficient

of determinations. As can be observed from Figure 9 and the values of the coefficient of determination, see Table 5, the curves give a good presentation for the data points.

Table 5. The parameter values for the curves and the coefficient of determination.

	C [N/m]	a	s [m]	R^2
Bow shoulder	2717.976	0.56	0.014	0.865
Midship	2402.378	0.583	0.014	0.933

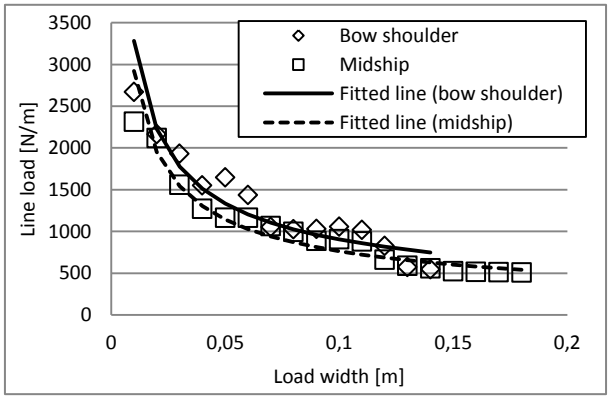

Figure 11. Maximum line load defined starting from the hotspot and then expanding to the neighbouring sensors following the line load.

Line load on the pusher plates

The measured maximum line loads are next determined from the pusher plates. As described above the pusher plates used in the tests were 2.4 meters long. Three of the pusher plates were producing reliable data as the fourth, the one closest to the ending point of test line, had connection problems during the second test series. The maximum line load for a load width of 2.4 meters was determined by studying the time histories of the pushing plates 1, 2 and 3 separately during the closing channel tests in the second test series. The maximum line load for a load width of 2.4 meters was determined to be the measured maximum on a single pusher plates.

The maximum line load for a width of 5 meters was determined by calculating the line loads for two adjacent pusher plates. It was assumed that the plates carry the loading over the gap between the plates. Following this method, two time histories were produced for each test runs. One time history was determined with pusher plates 1 and 2 and one with the pusher plates 2 and 3. The maximum line load occurring in these time histories was the maximum line load for a load width of 5 meters. The maximum line load for a width of 7.5 meters was determined using the same method, but calculating the time history using all three pusher plates.

Figure 12 presents the maximum line loads measured on pusher plates using the described method. In the closing channel test, the moving ice sheet on the starboard side of the model started to raft with the immobile ice sheet on the port side of the model during the test as the channel closed before the model reached the end of the test line. Therefore, the maximum line loads on the pusher plates are determined for the whole duration of the tests and for the time before the channel started to raft. The pusher plate data is gathered from the test runs 3 to 6 in the second test series; the same tests as the pressure foil data presented in above. Furthermore, the line load curves for the bow shoulder and midship are presented for comparison in Figure

11. The line load curves for the bow shoulder and midship are determined with Equation (3) and using the parameter values presented in Table 5.

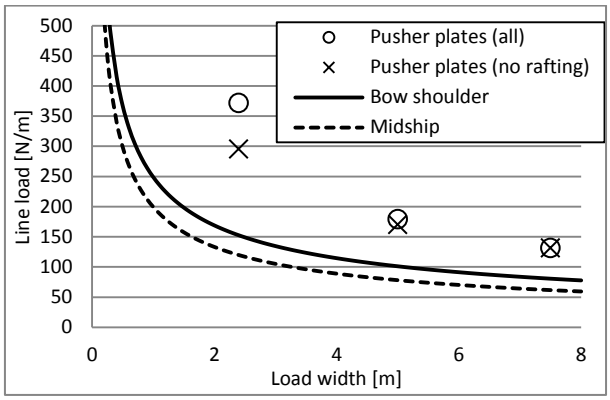

Figure 12. The maximum line load measured on pusher plates during the second test series and the line load curves for the bow shoulder and midship as a function of load width.

It can be observed from Figure 12 that the line load produced to the ice sheet is higher than the line loads occurring on the ship model hull. The difference is more significant in narrower load widths, but the line loads measured with pusher plates are approaching the line loads measured on the model hull in greater load widths. Comparison of the pusher plate data from the time before the ice sheets started to raft and the data from the whole test time shows that the line load is clearly smaller in a narrower load width when no rafting happens. When the load width is increased, the measured maxima, with and without rafting, are approaching and with a load width of 7.5 meters, the highest maximum is measured before the rafting occurs.

Comparison to earlier study

Kujala and Arughadhoss (2012) conducted a similar study with the models of Uikku and a general cargo ship. They defined the curves for the line load as a function of load widths for the bow of Uikku and the midship of the general cargo ship. As the curve for the midship has been presented in this paper, the results will be compared next. The scale used by Kujala and Arughadhoss in the model tests was 31.56 for the general cargo ship. In their study, *s* was set to 0.011 meters and using non-linear least mean square method, the parameters *C* and *a* obtained values of 1552 [N/m] and 0.76 respectively. As the model tests were conducted with different scales, the results are scaled into a full scale, see Figure 13. As can be seen from Figure 13, the results of the two studies are comparable and the difference is insignificant.

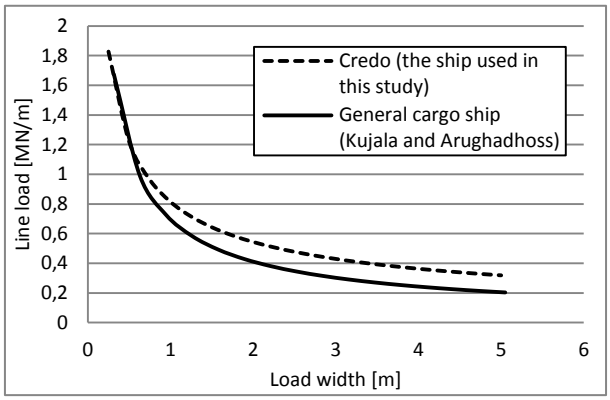

Figure 13. Comparison of the results at the midship of this study and the study conducted by Kujala and Arughadhoss (2012). The line load scaled into a full scale.

DISCUSSION

The study showed that the load panel and the pressure foil measurements correlate well. This indicates that the measurements conducted with the foils are reliable. In addition it was shown that the number of load cases of smaller load width is highly dependent on the chosen threshold value. These findings suggest that the load cases having a small load width contain many cases where the line load and the pressure in single load cells are low.

Smaller loads could be due to broken ice pieces having contact with the foil. After the ice piece has broken from the ice sheet, it hits the foil resulting in plenty of smaller ice loads with a narrow width. Another explanation for the large number of minor ice loads, could be that the ice is not breaking through crushing, especially at the bow shoulder area, the hull shape is not parallel to the ice sheet which enables the ice to break through bending and shear failure. If the ice breaks through bending or shear failure, the measured loadings are smaller than when it would have broken through crushing.

The study with the line loads determined from the total force affecting the contact line showed that the average line load is increasing in the smaller values of the load width, reaching the maximum with the contact widths of 0.05 to 0.1 meters. When the total contact length of the line load is narrow, less than 0.05 meters, the occurring maximum line loads are low in the majority of the loading cases. This would suggest that the load width needs to be wide enough (on average) that the loading process can be a fully developed loading case and the possibility of maximum local ice load to occur is high. The fully developed loading case refers here to the cases where the ice is broken through the failure mode resulting the highest possible loads. At midship this would be through crushing and at the bow shoulder through bending.

The effect of the contact width on the maximum possible line load study (the study where the line loads were defined starting from the hot spot and then expanding to the neighbourhood) gave expected results. The maximum line load is decreasing as a function of the contact width at the bow shoulder and midship. The fitted curves give good presentation from the data points and are comparable to the earlier studies.

The study on the line loads induced to the ice sheet showed similar behaviour as the line load on the ship model's hull, as the maximum line load is decreasing as a function of load width. The comparison of line loads induced to the ice sheet and measured on the hull showed that the line loads inserted into the ice sheet are higher. The maxima for the pusher plates were determined for the whole duration of the tests and for the times in the tests before rafting occurred. Study of the maxima showed that the measured maximum in a smaller loading width is clearly higher when rafting occurs. With wider loading widths, the difference decreases and with a loading width of 7.5 meters the highest maximum occurs before the rafting starts. Therefore, the rafting ice might have carried some of the loading.

In addition to rafting, the movement of the model in relation to the crushing ice sheet can result in smaller loading. As the model moves, the ice is not piling against the model's hull and the contact area cannot increase in height. Vice versa, the pushing plates were not moving in relation to the pushed ice sheet, which enables the crushing ice to pile and the nominal contact to increase and the total loading capacity of ice to increase. Some piling was observed against the pusher plates during the tests, but it was not considered significant. Because the line load on pusher plates was measured with load sensors the increase in contact height on the plates was not able to study.

ACKNOWLEDGEMENT

The model tests presented in this paper were conducted within EU FP7 project called SAFEWIN. The funding came from European Commission and the line drawings of the ship model were received from FKAB. Their contributions are gratefully acknowledged. Furthermore the writers want to thank all the project partners AS2CON, Arctic and Antarctic Research Institute, Finnish Meteorological Institute, Finnish Transport Agency, ILS Oy, Stena Rederi AB, Swedish Maritime Administration, Swedish Meteorological and Hydrological Institute, Tallinn University of Technology and AS Tallink Group. Special thanks to the staff of Aalto University. Writers would like to thank Jesse Lehtonen and Lauri Kuuliala for their help in data processing. The support from VTT personnel Kari Kolari and Pieti Marjavaara is also recognized.

REFERENCES

Kujala, P., Goldstein, R., Osipenko, N., Danilenko, V., 1991. "A Ship in Compressive Ice, Preliminary Model Test Results and Analysis of the Process" Report from the joint Finnish-Soviet research project, Otaniemi, M-111 63p.

Kujala, P., Suominen, M., Riska, K., 2009. Statistics of Ice Loads Measured on MT Uikku in the Baltic. Proceedings of the 20th International Conference on Port and Ocean Engineering under Arctic Conditions, POAC09-51, Luleå, Sweden.

Kujala , P., Arughadhoss, S., 2012. Statistical analysis of ice crushing pressures on a ship's hull during hull-ice interaction. Cold Regions Science and Technology 70 (2012) 1-11.

Riska, K., Kujala, P., Goldstein, R., Danilenko, V., Osipenko, N., 1995. Application of Results From the Research Project "A Ship in Compressive Ice" to ship operability. POAC'95, (1995) Vol 4, 84–99.

Suominen, M., Kujala, P., 2012. Ice Model Tests in Compressive Ice. 21st IAHR International Symposium on Ice, Dalian, China, June 11 to 15, 2012